Supplementary Material

Promoting the reversibility of electrolytic MnO_2-Zn battery with high areal capacity by $VOSO_4$ mediator

Yong Xu, Wenjie Huang, Jun Liu, Renzong Hu, Liuzhang Ouyang, Lichun Yang*, Min Zhu

School of Materials Science and Engineering, and Guangdong Provincial Key Laboratory of Advanced Energy Storage Materials, South China University of Technology, Guangzhou 510640, Guangdong, China.

Correspondence to: Prof./Dr. Lichun Yang, School of Materials Science and Engineering, and Guangdong Provincial Key Laboratory of Advanced Energy Storage Materials, South China University of Technology, 381 Wushan Road, Tianhe District, Guangzhou 510640, China. E-mail: mslcyang@scut.edu.cn

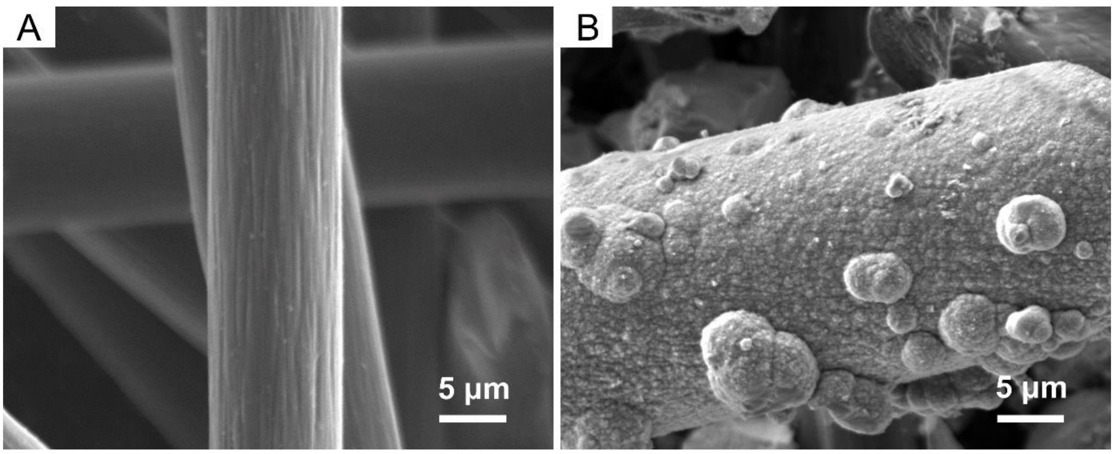

Supplementary Figure 1. The SEM images of (A) the pure carbon felt and (B) the carbon felt electrode after 30 cycles in E-Mn at 5 mAh cm^{-2} and 10 mA cm^{-2}.

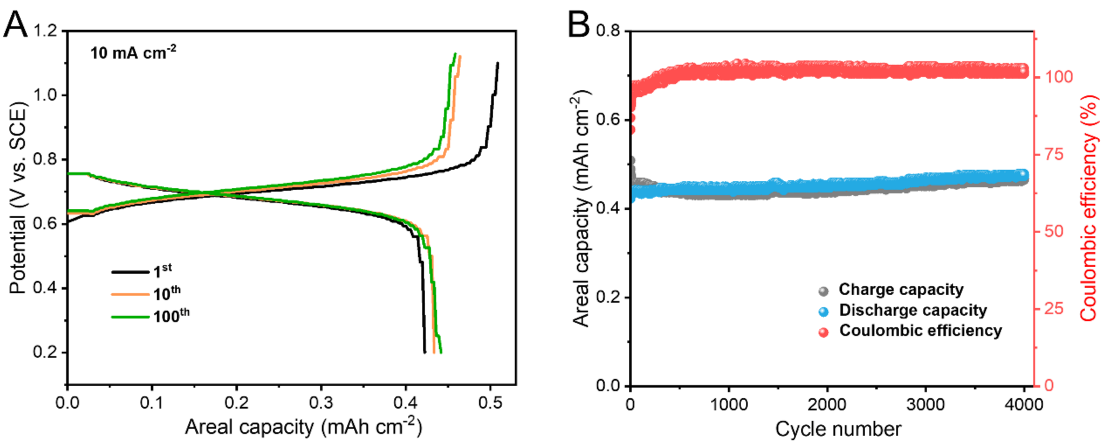

Supplementary Figure 2. (A) Charge-discharge curves and (B) cycling performance of E-VO at 10 mA cm^{-2}.

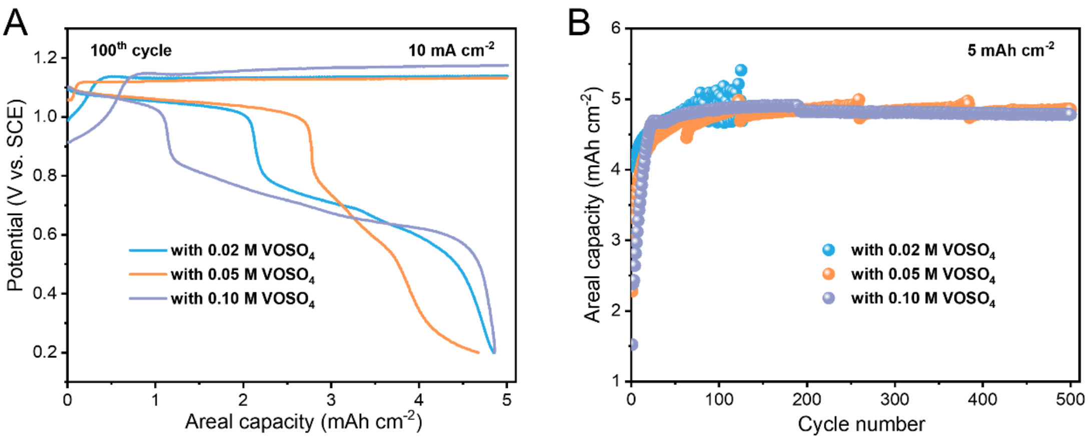

Supplementary Figure 3. (A) Charge/discharge curves and (B) cycling performance of E-Mn with different $VOSO_4$ at 10 mA cm^{-2}.

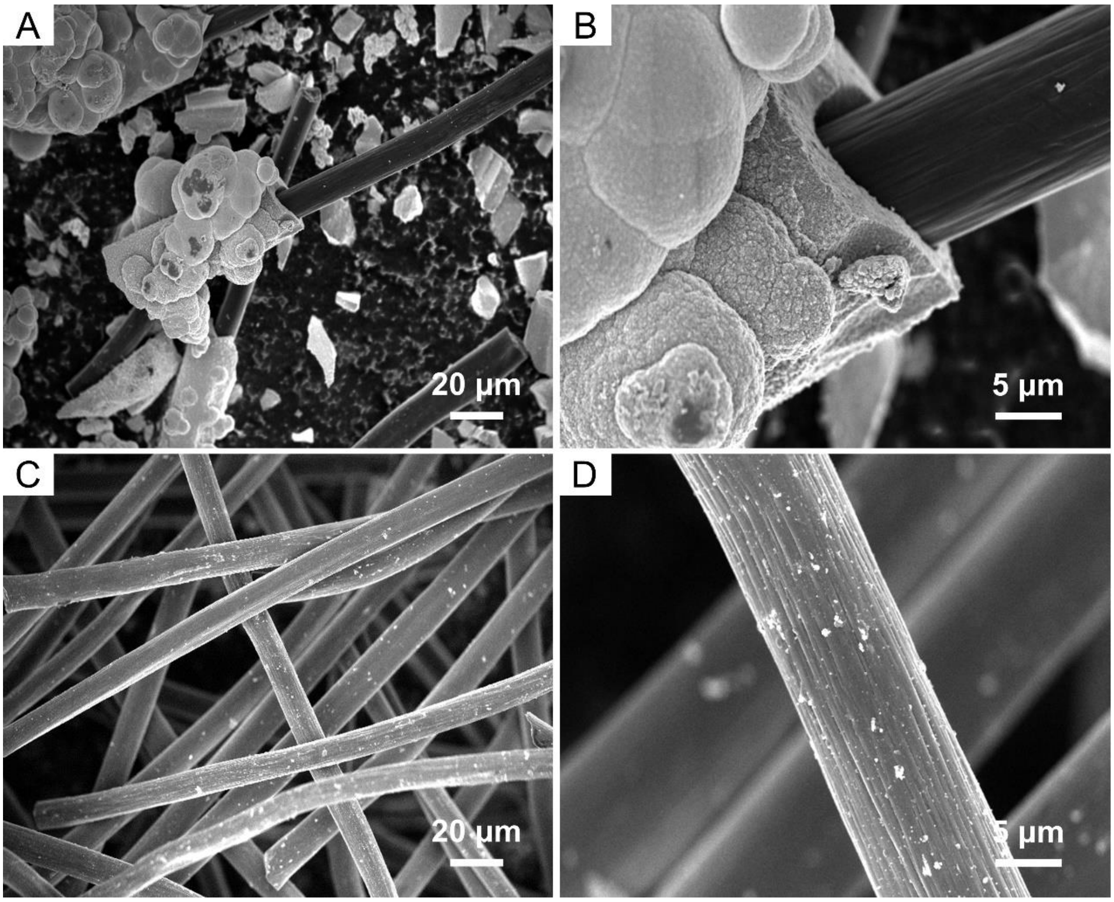

Supplementary Figure 4. SEM images of the carbon felt tested in (A, B) E-Mn and (C, D) E-MnVO after 200 cycles of charge/discharge at 5 mAh cm^{-2} and 10 mA cm^{-2}.

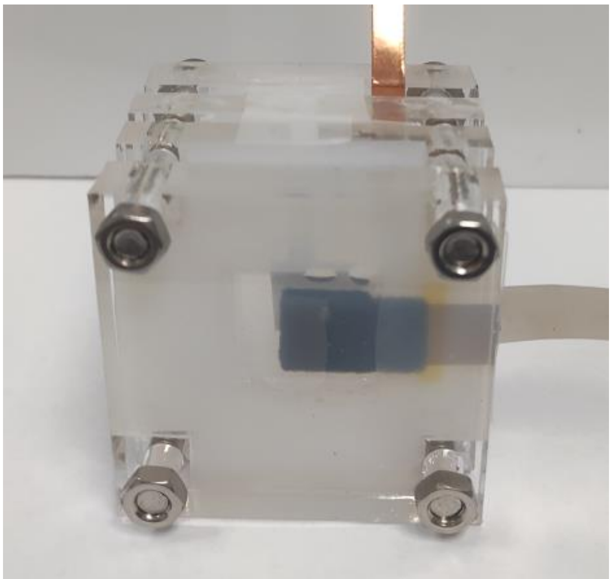

Supplementary Figure 5. Photo of the two-electrode configuration adopted for the test of the MnO_2-Zn, $VOSO_4$-Zn, and MnO_2/$VOSO_4$-Zn batteries.

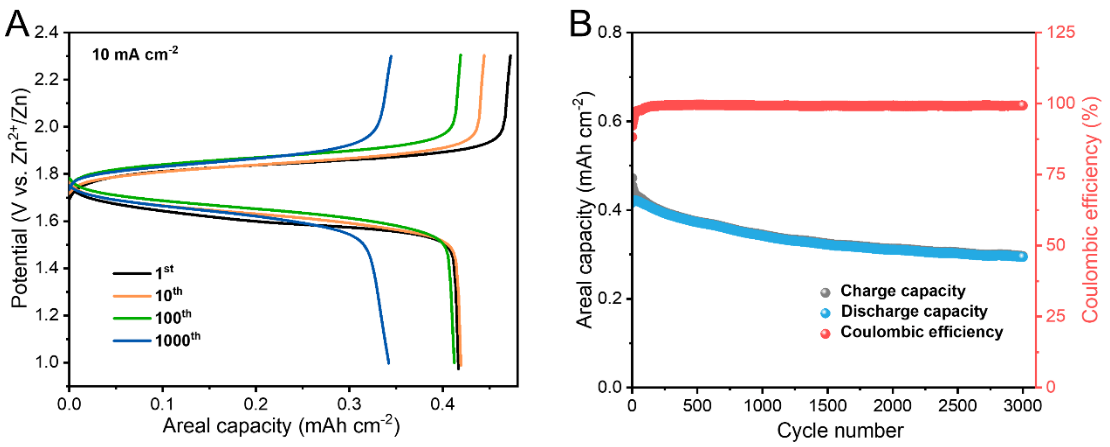

Supplementary Figure 6. (A) Charge/discharge curves and (B) cycling performance of the $VOSO_4$-Zn battery at 10 mA cm^{-2}.

To quantify the capacity contribution of $VOSO_4$ in the MnO_2/$VOSO_4$-Zn battery, the galvanostatic charge/discharge performance of the $VOSO_4$-Zn battery was tested in the voltage range of 1.0-2.3 V. At 10 mA cm^{-2}. The $VOSO_4$-Zn battery displays stable charge/discharge platforms at around 1.84/1.61 V, delivering a charge/discharge capacity of 0.47/0.4 mAh cm^{-2} in the initial cycle. The reversible capacity maintains 0.3 mAh cm^{-2} after 3000 cycles, displaying good cyclic stability.

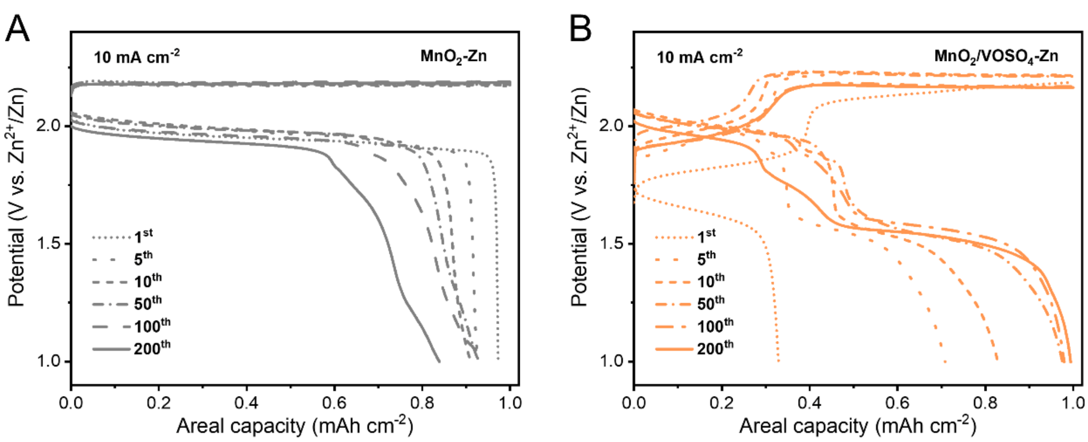

Supplementary Figure 7. Charge/discharge curves of (A) MnO_2-Zn and (B) MnO_2/$VOSO_4$-Zn batteries at 1 mAh cm^{-2} and 10 mA cm^{-2}.

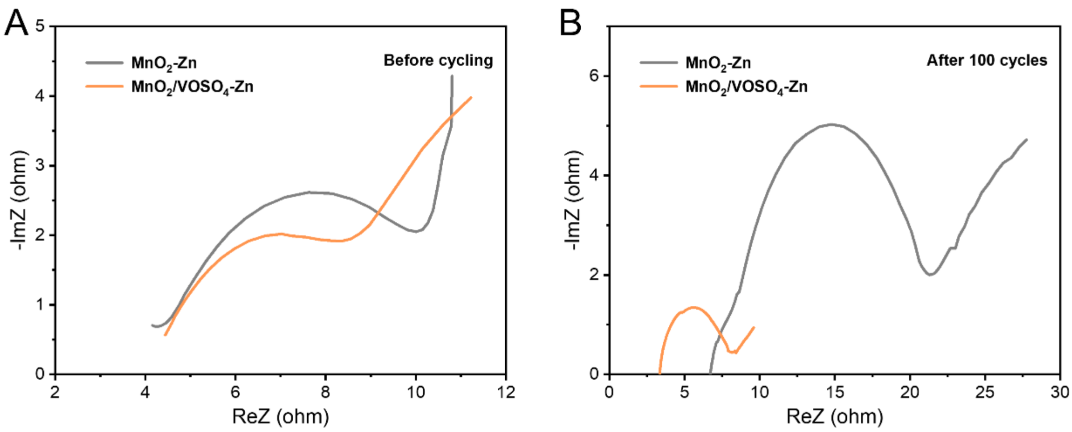

Supplementary Figure 8. Nyquist plots of the MnO_2-Zn and $MnO_2/VOSO_4$-Zn batteries (A) before cycling and (B) after 100 cycles.

The ohmic resistance (R_s) and charge transfer resistance (R_{ct}) of the MnO_2-Zn battery significantly increase after 100 cycles of charge/discharge, indicating more MnO_2 particles are accumulated on the carbon felt.

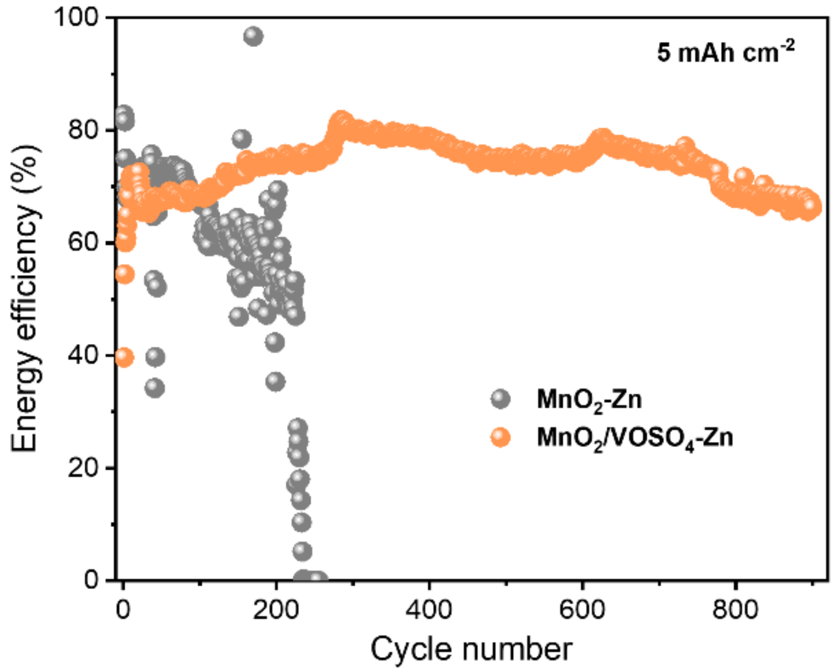

Supplementary Figure 9. Energy efficiency of the MnO_2-Zn and $MnO_2/VOSO_4$-Zn batteries charged/discharged at 5 mAh cm^{-2} and 10 mA cm^{-2}.

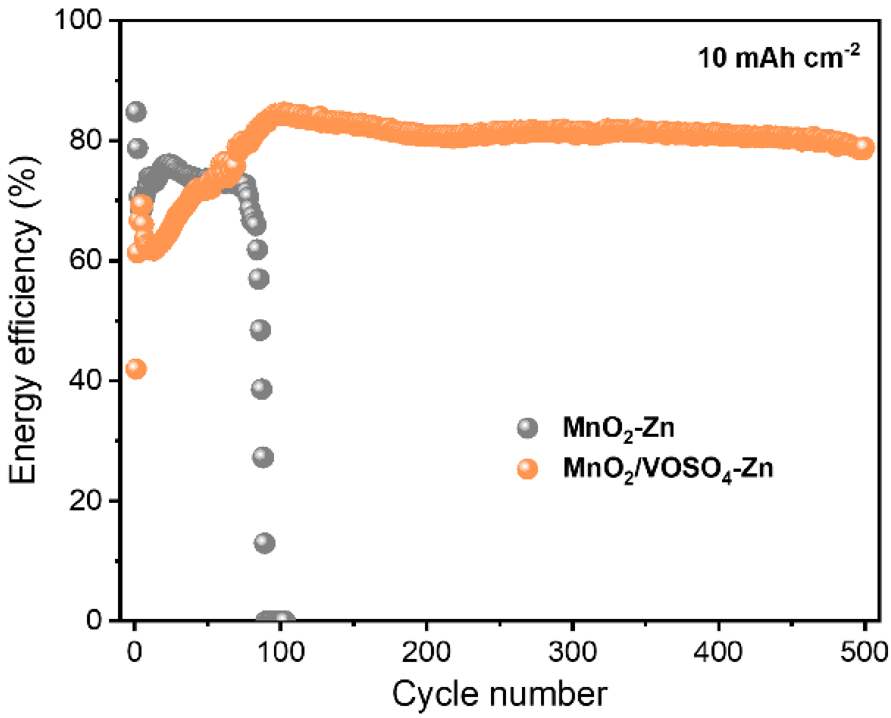

Supplementary Figure 10. Energy efficiency of the MnO_2-Zn and $MnO_2/VOSO_4$-Zn batteries charged/discharged at 10 mAh cm^{-2} and 10 mA cm^{-2}.

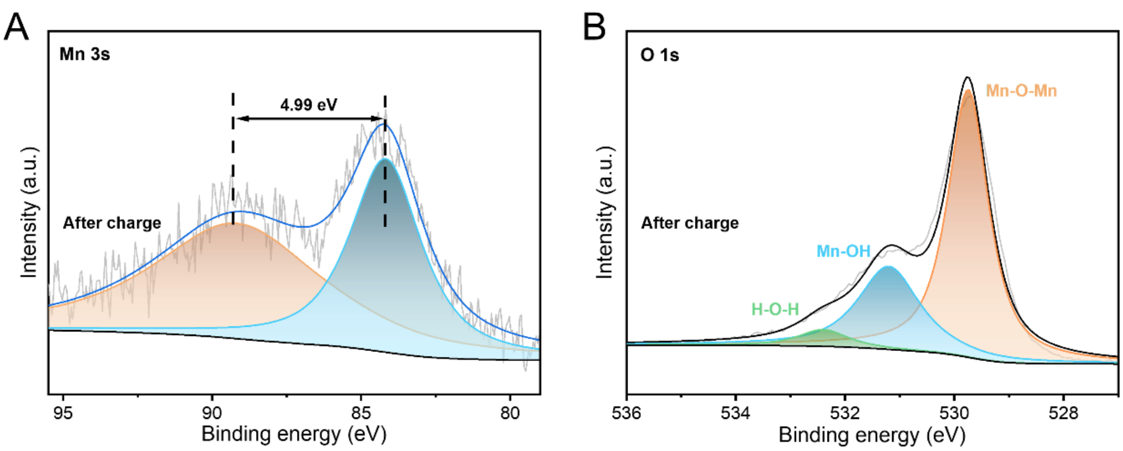

Supplementary Figure 11. (A) Mn 3s and (B) O 1s peaks in the XPS spectrum of the cathode from the MnO_2-Zn battery after the 20th charging.

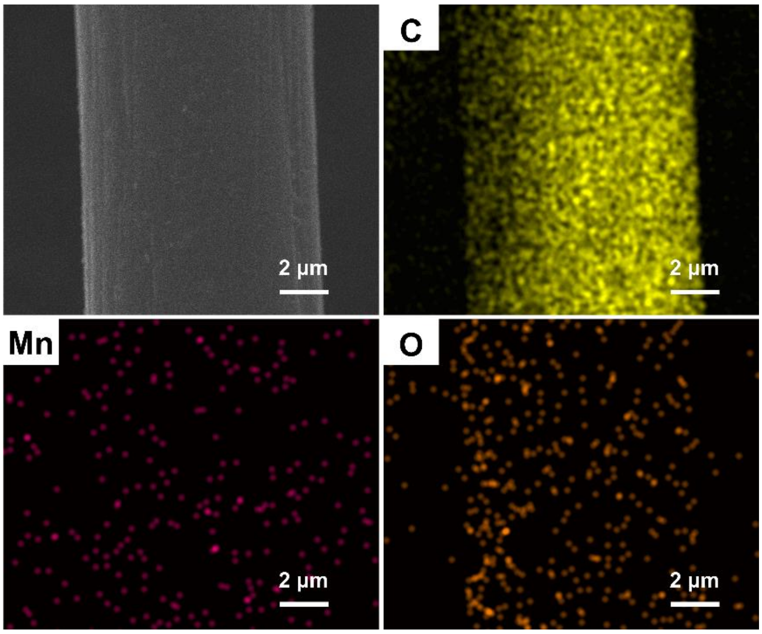

Supplementary Figure 12. EDS elemental mapping of the carbon felt in the $MnO_2/VOSO_4$-Zn battery after the 20th discharge process.

The surface of the carbon felt from the $MnO_2/VOSO_4$-Zn battery is similar to the pristine state. And the signal of Mn is very weak and spreads through the whole image, suggesting the residual of MnO_2 is very low and the signal is probably related with noise.

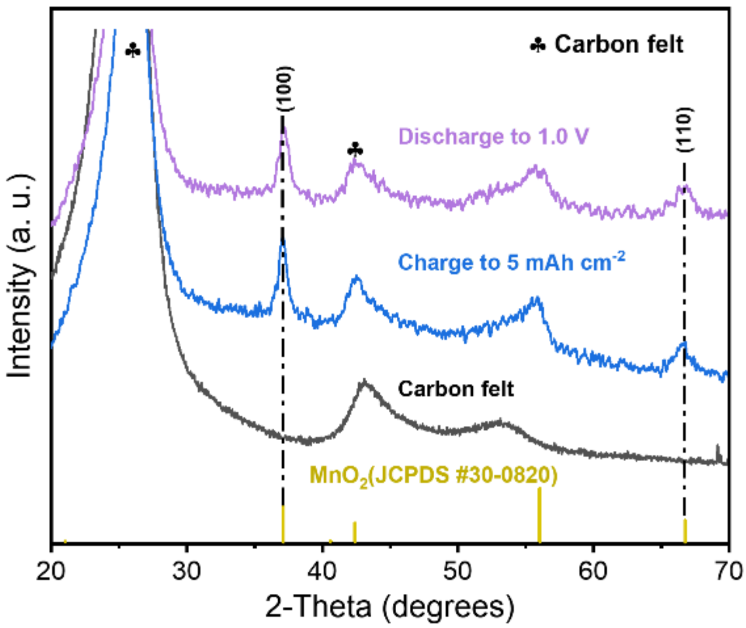

Supplementary Figure 13. XRD patterns of the cathode from the MnO_2-Zn battery after the 20^{th} charging and discharging at 5 mAh cm^{-2} and 10 mA cm^{-2}.

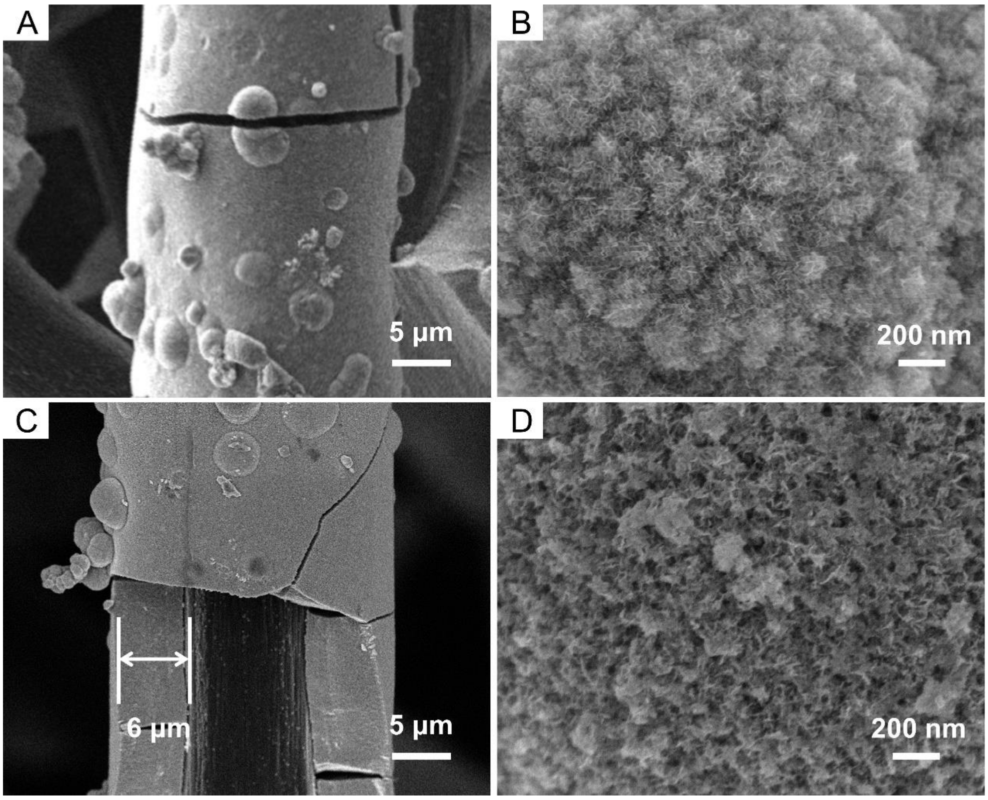

Supplementary Figure 14. SEM images of the cathode from the MnO_2-Zn battery after the 20th (A, B) charging and (C, D) discharging at 5 mAh cm^{-2} and 10 mA cm^{-2}.

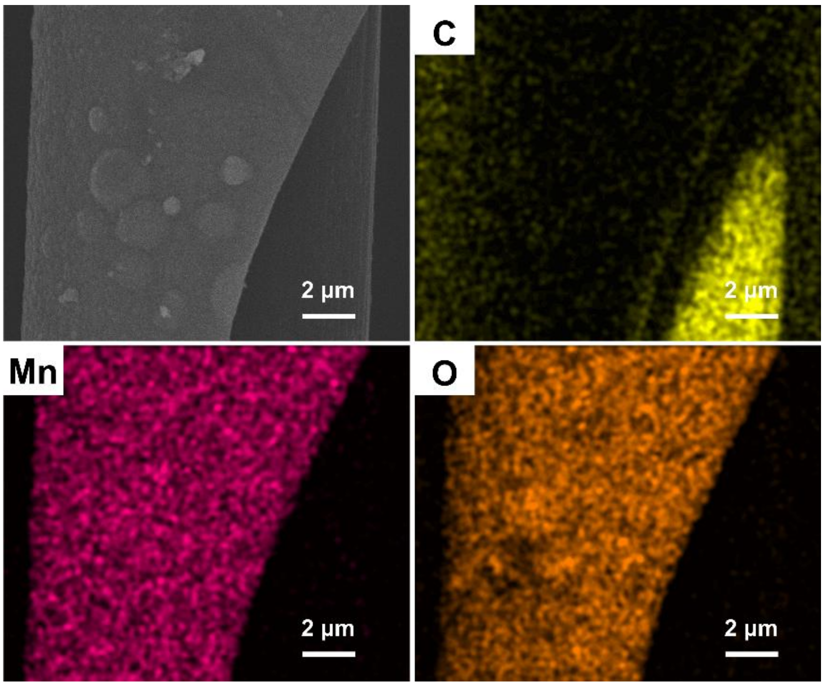

Supplementary Figure 15. EDS elemental mapping of the carbon felt in the MnO_2-Zn battery after the 20th discharge process.

A coating layer can be observed on the carbon felt from the MnO_2-Zn battery, and intensive signals of Mn and O can be detected on the coating, indicating the composition of the coating is MnO_2.

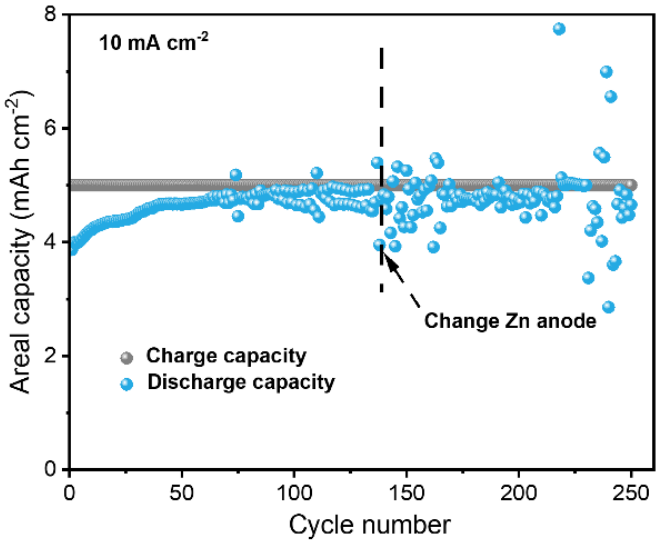

Supplementary Figure 16. Cyclic performance of the MnO_2-Zn battery tested before and after changing zinc foil at 5 mAh cm^{-2} and 10 mA cm^{-2}.

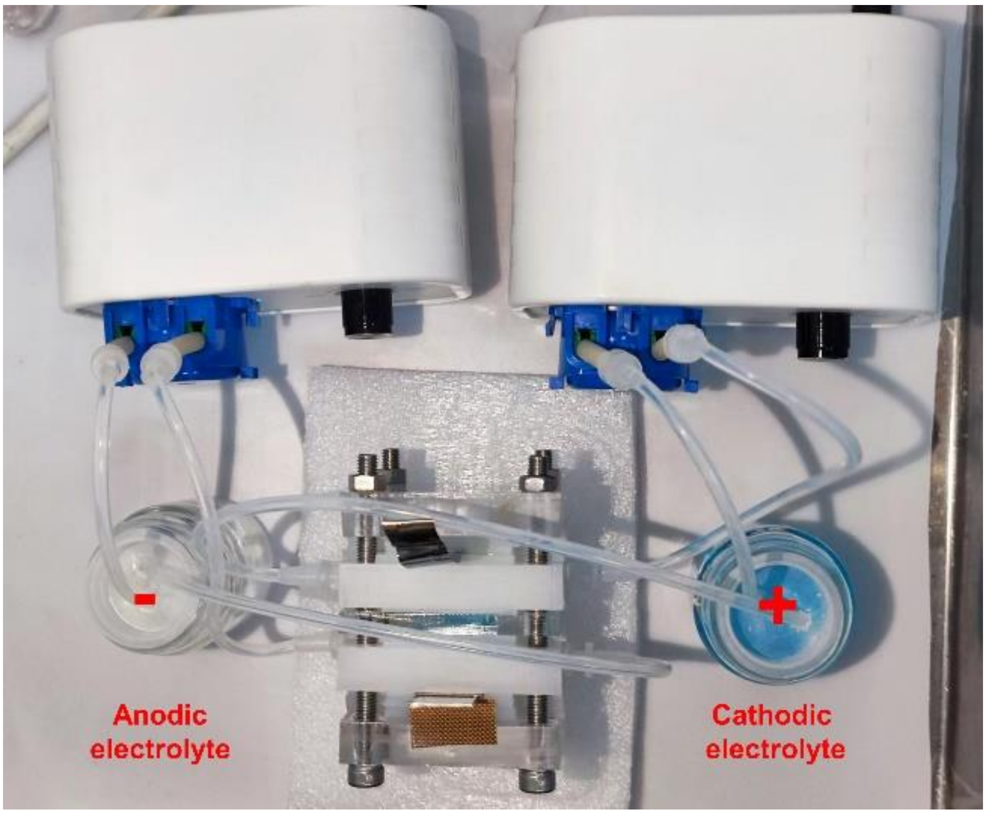

Supplementary Figure 17. Optical image of MnO_2/$VOSO_4$-Zn flow battery.

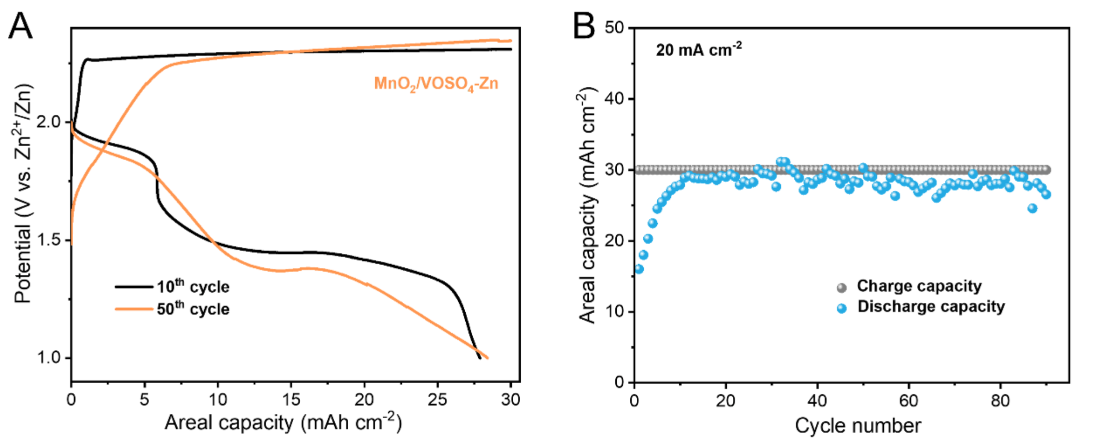

Supplementary Figure 18. (A) Charge/discharge voltage profiles and (B) cycling performance of the $MnO_2/VOSO_4$-Zn flow battery tested at 30 mAh cm^{-2} and 20 mA cm^{-2}.

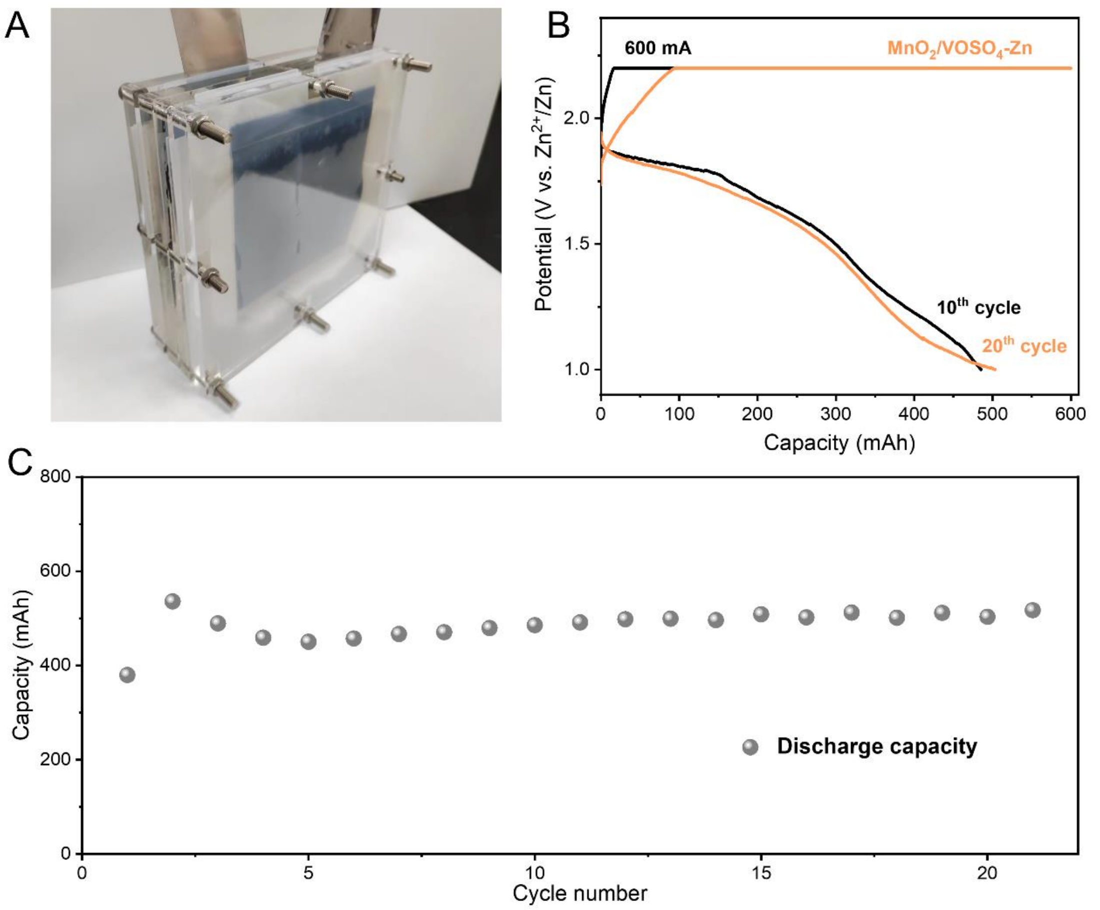

Supplementary Figure 19. (A) Optical picture, (B) charge/discharge profiles, and (C) cycling performance of the scale-up $MnO_2/VOSO_4$-Zn battery tested at 600 mAh and 600 mA cm^{-2}.

Supplementary Table 1. Electrochemical performance of the reported MnO_2-Zn batteries.

Strategy	Charge capacity ($mAh\ cm^{-2}$)	Average coulombic efficiency (%)	Cycles	Ref.
$VOSO_4$ mediator	**5** **10** **20 (flow battery)**	**98** **97** **97**	**900** **500** **300**	**This work**
Bromice mediator	6.67	93	600	[1]
Iodide mediator	2.5	100	400	[2]
MOFs as the electrodeposition surface	0.17	100	1000	[3]
Acid-alkaline dual electrolyte	0.5	98.4	1500	[4]
Regulation of sulfuric acid	2	96	1800	[5]
Amino acid additives	2 (flow battery)	-	1000	[6]
Acetate anion chemistry	2	98	200	[7]
High-concentration dual-complex electrolyte	10	96	200	[8]
Al^{3+} Addition	2	100	2000	[9]
Salt bridge gel electrolyte	1.35	94.8	350	[10]
Electrolyte-decoupling	-	96	200 h (500 mA g^{-1})	[11]
Ni^{2+} catalyst	1	99.9	450	[12]
Proton-trapping agent	1	96	1000	[13]
Phosphate proton reservoir	0.99	99	3000	[14]
PH-Buffer	0.8	99.6	2000	[15]

REFERENCES

1. Zheng X, Wang Y, Xu Y, et al. Boosting Electrolytic MnO2–Zn Batteries by a Bromine Mediator. Nano Lett. 2021;21: 8863-8871. [DOI: 10.1021/acs.nanolett.1c03319]
2. Lei J, Yao Y, Wang Z, Lu Y-C. Towards high-areal-capacity aqueous zinc–manganese batteries: promoting MnO2 dissolution by redox mediators. Energy Environ. Sci. 2021;14: 4418-4426. [DOI: 10.1039/d1ee01120k]
3. Gou L, Li J, Liang K, Zhao S, Li D, Fan X. Bi-MOF Modulating MnO2 Deposition Enables Ultra-Stable Cathode-Free Aqueous Zinc-Ion Batteries. Small 2023;19: 2208233. [DOI: 10.1002/smll.202208233]
4. Liu C, Chi X, Han Q, Liu Y. A High Energy Density Aqueous Battery Achieved by Dual Dissolution/Deposition Reactions Separated in Acid-Alkaline Electrolyte. Adv. Energy Mater. 2020;10: 1903589. [DOI: 10.1002/aenm.201903589]
5. Chao D, Zhou W, Ye C, et al. An Electrolytic Zn–MnO2 Battery for High-Voltage and Scalable Energy Storage. Angew. Chem. Int. Ed. 2019;58: 7823-7828. [DOI: 10.1002/anie.201904174]
6. Liu Y, Nan M, Zhao Z, et al. Manganese-based flow battery based on the MnCl2 electrolyte for energy storage. Chem. Eng. J. 2023;465: 142602. [DOI: 10.1016/j.cej.2023.142602]
7. Zeng X, Liu J, Mao J, et al. Toward a Reversible Mn4+/Mn2+ Redox Reaction and Dendrite-Free Zn Anode in Near-Neutral Aqueous Zn/MnO2 Batteries via Salt Anion Chemistry. Adv. Energy Mater. 2020;10: 1904163. [DOI: 10.1002/aenm.201904163]
8. Huang J, Chi X, Wu J, Liu J, Liu Y. High-concentration dual-complex electrolyte enabled a neutral aqueous zinc-manganese electrolytic battery with superior stability. Chem. Eng. J. 2022;430: 133058. [DOI: 10.1016/j.cej.2021.133058]
9. Qin Z, Song Y, Yang D, et al. Enabling Reversible MnO2/Mn2+ Transformation by Al3+ Addition for Aqueous Zn–MnO2 Hybrid Batteries. ACS Appl. Mater. Interfaces 2022;14: 10526-10534. [DOI: 10.1021/acsami.1c22674]
10. Xu Q, Xie Q-X, Xue T, et al. Salt Bridge-intermediated three phase decoupling electrolytes for high voltage electrolytic aqueous Zinc-Manganese dioxides battery. Chem. Eng. J. 2023;451: 138775. [DOI: 10.1016/j.cej.2022.138775]
11. Zhong C, Liu B, Ding J, et al. Decoupling electrolytes towards stable and high-energy rechargeable aqueous zinc–manganese dioxide batteries. Nat. Energy 2020;5: 440-

449. [DOI: 10.1038/s41560-020-0584-y]

12. Chao D, Ye C, Xie F, et al. Atomic Engineering Catalyzed MnO2 Electrolysis Kinetics for a Hybrid Aqueous Battery with High Power and Energy Density. Adv. Mater. 2020;32: 2001894. [DOI: 10.1002/adma.202001894]
13. Sun J, Liu Z, Li K, et al. Proton-Trapping Agent for Mitigating Hydrogen Evolution Corrosion of Zn for an Electrolytic MnO2/Zn Battery. ACS Appl. Mater. Interfaces 2022;14: 51900-51909. [DOI:10.1021/acsami.2c14370]
14. Liu Y, Qin Z, Yang X, Liu J, Liu X-X, Sun X. High-Voltage Manganese Oxide Cathode with Two-Electron Transfer Enabled by a Phosphate Proton Reservoir for Aqueous Zinc Batteries. ACS Energy Lett. 2022;7: 1814-1819. [DOI:10.1021/acsenergylett.2c00777]
15. Liu Z, Yang Y, Liang S, Lu B, Zhou J. pH-Buffer Contained Electrolyte for Self-Adjusted Cathode-Free Zn–MnO2 Batteries with Coexistence of Dual Mechanisms. Small Struct. 2021;2: 2100119. [DOI:10.1002/sstr.202100119]